

Optoelectronic Control of Atomic Bistability with Graphene

Mikkel Have Eriksen¹, Jakob E. Olsen², Christian Wolff¹, and Joel D. Cox^{1,3,*}

¹Center for Nano Optics, University of Southern Denmark, Campusvej 55, DK-5230 Odense M, Denmark

²Faculty of Engineering, University of Southern Denmark, Campusvej 55, DK-5230 Odense M, Denmark

³Danish Institute for Advanced Study, University of Southern Denmark, Campusvej 55, DK-5230 Odense M, Denmark

 (Received 22 July 2022; accepted 17 November 2022; published 16 December 2022)

We explore the emergence and active control of optical bistability in a two-level atom near a graphene sheet. Our theory incorporates self-interaction of the optically driven atom and its coupling to electromagnetic vacuum modes, both of which are sensitive to the electrically tunable interband transition threshold in graphene. We show that electro-optical bistability and hysteresis can manifest in the intensity, spectrum, and quantum statistics of the light emitted by the atom, which undergoes critical slow-down to steady state. The optically driven atom-graphene interaction constitutes a platform for active control of driven atomic systems in coherent quantum control and atomic physics.

DOI: [10.1103/PhysRevLett.129.253602](https://doi.org/10.1103/PhysRevLett.129.253602)

Coherent optical control of atomic systems enables fundamental explorations of quantum physics while promising disruptive applications in diverse fields, ranging from information and communication technologies to optical sensing and metrology [1]. In this context, nanophotonic architectures that enhance atom-photon interactions offer a robust and scalable platform for developing next-generation integrated photonic devices [2,3]. Metal nanostructures supporting plasmons—collective excitations in the free electron plasma—have been widely explored as subwavelength light-focusing elements in hybrid systems, where the combined broad spectral response of a plasmonic resonator and the narrow linewidth of a few-level quantum light emitter (e.g., a quantum dot) are predicted to enable phenomena such as nonlinear Fano effects [4,5], optical bistability [6–8], optical hysteresis [9–11], excitonic population transfer [12], and enhanced resonance fluorescence [13,14]; a salient feature in these systems are nonlinear dynamics emerging from the atom self-interaction mediated by plasmon resonances.

While plasmons in noble metals facilitate nanoscopic light focusing, they suffer from large intrinsic Ohmic loss and cannot easily be tuned in an active manner. These limitations are partly alleviated in highly doped graphene, which hosts long-lived and actively tunable plasmon resonances that strongly concentrate light [15], thus presenting new opportunities to control atom-light interactions on the nanoscale [16–19]. Unfortunately, achievable Fermi levels $E_F \lesssim 1$ eV restrict graphene plasmon resonances to the terahertz and infrared spectral range lying well below the operational frequencies of robust quantum light sources [20,21]. Nevertheless, the carbon monolayer exhibits an impressive light-matter interaction associated with optical excitation of electrons between conical valence and conduction bands, giving rise to a broadband 2.3% light

absorption at energies beyond the electrically tunable $2E_F$ threshold [22,23]. In the context of coherent optical control, recent experiments confirm that optoelectronic tunability of the graphene interband response can be harnessed to manipulate quantum light emission [24,25], also enabling fast dynamical control of strong near-field interactions that produce $\gtrsim 1000$ -fold enhancement in the decay rate of erbium emitters [26].

Considerable efforts have been made to electrically control quantum light generation using graphene, while few investigations have explored *optically driven* atomic systems in such an actively tunable nanophotonic environment [11,18]. In particular, changes in the local photonic density of states experienced by an atom in the spectral neighborhood of its transition frequency impact both the optically induced self-interaction and mesoscopic quantum electrodynamic phenomena manifesting from vacuum fluctuations [27], such as the Purcell effect [16] and Lamb shift [19]. The dynamics of a driven two-level atom (TLA) experiencing all the aforementioned phenomena is hitherto unexplored, even in studies of atom-plasmon interactions.

In this Letter, we theoretically explore the nonlinear response of an optically driven TLA near an electrically tunable graphene sheet that mediates optical and vacuum-induced light-matter interactions. We focus on bistability that emerges from the feedback of the optically induced atomic transition dipole produced by the carbon monolayer, which we demonstrate can be harnessed to actively switch the hybrid system into different metastable states. The interband transition threshold in the graphene sheet simultaneously impacts the spontaneous emission rate (Purcell effect) and atomic transition frequency (Lamb shift), leading to complex dynamics in the TLA response. Our findings motivate further studies of quantum electrodynamic

effects in atomic bistability, while offering a prescription for active and *in situ* modification of quantum states in optical lattices and integrated nanophotonic platforms.

We consider a generic TLA (e.g., an atom or quantum dot) positioned at $\mathbf{r} = (x, y, z)$ above a graphene sheet extended in the $z = 0$ plane and interfacing homogeneous dielectric media with permittivity ϵ_a above and ϵ_b below, respectively, as depicted schematically in Fig. 1(a). The TLA Hamiltonian is expressed as

$$\mathcal{H} = \hbar \sum_{j=1}^2 \epsilon_j |j\rangle \langle j| + \hbar \int_0^\infty d\omega \omega \int d^3 \mathbf{r}' \hat{\mathbf{f}}_\omega^\dagger(\mathbf{r}') \cdot \hat{\mathbf{f}}_\omega(\mathbf{r}) - \hat{\mathbf{d}} \cdot \left[\mathbf{E}(\mathbf{r}, \omega_L) e^{-i\omega_L t} + \int_0^\infty d\omega \hat{\mathbf{E}}_R(\mathbf{r}, \omega) + \text{H.c.} \right], \quad (1)$$

where the first term is the bare atom Hamiltonian comprised of states $|j\rangle$ with energies $\hbar \epsilon_j$ for $j \in \{1, 2\}$, the second term corresponds to the vacuum radiation field, expressed using bosonic field operators $\hat{\mathbf{f}}_\omega^\dagger$ ($\hat{\mathbf{f}}_\omega$) that create (annihilate) photons at frequency ω , and the final term describes the atom coupling with the classical monochromatic field $\mathbf{E} e^{-i\omega_L t} + \text{c.c.}$ and quantized radiation field operator $\hat{\mathbf{E}}_R$ through their projection on the dipole operator $\hat{\mathbf{d}}$ [13,18,28].

The classical field is comprised of the external field \mathbf{E}^{ext} , its reflection by the graphene sheet, and the field produced by the TLA dipole image in graphene, so that

$$\mathbf{E}(\mathbf{r}, \omega_L) = \frac{1}{\tilde{\epsilon}} [(1 + r_\omega) \mathbf{E}^{\text{ext}} + \omega_L^2 \mu_0 \mathcal{G}_\omega^{\text{ref}}(\mathbf{r}, \mathbf{r}) \cdot \langle \hat{\mathbf{d}} \rangle], \quad (2)$$

where the reflection coefficient $r_\omega = [\sqrt{\epsilon_b} - \sqrt{\epsilon_a} + \sigma_\omega / c\epsilon_0] / [\sqrt{\epsilon_b} + \sqrt{\epsilon_a} + \sigma_\omega / c\epsilon_0]$ for normally impinging light and the reflected part of the Green's tensor $\mathcal{G}_\omega^{\text{ref}}(\mathbf{r}, \mathbf{r}')$ that mediates the self-interaction of the dipole $\langle \hat{\mathbf{d}} \rangle$ ($\langle \dots \rangle$ denotes the quantum mechanical average) depend on the graphene surface conductivity σ_ω as explained in the Supplemental Material [29], while the prefactor $\tilde{\epsilon}^{-1}$ accounts for possible dielectric screening by the internal structure of the TLA relative to its host environment [9].

The quantum field operator of the inhomogeneous photonic environment is expressed in terms of the total classical Green's tensor \mathcal{G}_ω as [18,39]

$$\hat{\mathbf{E}}_R(\mathbf{r}, \omega) = i \sqrt{\frac{\hbar \omega^2}{\pi \epsilon_0 c^2}} \int d^3 \mathbf{r}' \sqrt{\text{Im}\{\chi_\omega(\mathbf{r}')\}} \mathcal{G}_\omega(\mathbf{r}, \mathbf{r}') \cdot \hat{\mathbf{f}}_\omega(\mathbf{r}'), \quad (3)$$

where χ is the susceptibility of the dielectric background. Following the procedure described in the Supplemental Material [29], we trace over the photonic reservoir to form a master equation for the density matrix $\hat{\rho}$ governing the TLA dynamics in the interaction picture:

$$\dot{\hat{\rho}} = -\frac{i}{\hbar} [\mathcal{V} + \hbar \delta \omega |2\rangle \langle 2|, \hat{\rho}] + \frac{\Gamma}{2} (|2\rangle \langle 1| \langle 2| \hat{\rho} |2\rangle \langle 1| - |2\rangle \langle 2| \langle \hat{\rho} - \hat{\rho} |2\rangle \langle 2|), \quad (4)$$

where

$$\mathcal{V} = -[\mathbf{d} \cdot \mathbf{E}(\mathbf{r}, \omega_L) e^{-i\omega_L t} + \text{c.c.}] (|1\rangle \langle 2| e^{-i\epsilon t} + \text{H.c.}) \quad (5)$$

is the atom-light interaction Hamiltonian,

$$\Gamma = \Gamma_0 + \frac{2\mu_0}{\hbar} \epsilon^2 \text{Im}\{\mathbf{d} \cdot \mathcal{G}_\epsilon^{\text{ref}}(\mathbf{r}, \mathbf{r}) \cdot \mathbf{d}\} \quad (6)$$

is the spontaneous emission rate, with $\Gamma_0 = \epsilon^3 |\mathbf{d}|^2 / 3\pi \epsilon_0 \hbar c^3$ denoting the vacuum emission rate [40], and

$$\delta \omega = \frac{\mu_0}{\pi \hbar} \mathcal{P} \int_0^\infty d\omega \omega^2 \frac{\mathbf{d} \cdot \text{Im}\{\mathcal{G}_\omega^{\text{ref}}(\mathbf{r}_0, \mathbf{r}_0)\} \cdot \mathbf{d}}{\epsilon - \omega} \quad (7)$$

quantifies the Lamb shift as a Cauchy principal value integral. In Eqs. (5)–(7), we have introduced the atomic transition frequency $\epsilon \equiv \epsilon_2 - \epsilon_1$ and transition dipole moment $\mathbf{d} \equiv \langle 1 | \hat{\mathbf{d}} | 2 \rangle = \langle 2 | \hat{\mathbf{d}} | 1 \rangle$. Inserting the Hamiltonian of Eq. (1) into Eq. (4) and writing $\langle \hat{\mathbf{d}} \rangle = \text{Tr}\{\hat{\mathbf{d}} \hat{\rho}\} = \mathbf{d} \rho_{21} + \text{c.c.}$, we obtain the familiar equations of motion for the density matrix elements $\rho_{jj'}$ = $\langle j | \hat{\rho} | j' \rangle$ in the rotating-wave approximation:

$$\dot{\rho}_{11} = \Gamma \rho_{22} + i(\Omega^* + G^* \tilde{\rho}_{12}) \tilde{\rho}_{21} - i(\Omega + G \tilde{\rho}_{21}) \tilde{\rho}_{12}, \quad (8a)$$

$$\dot{\tilde{\rho}}_{21} = (i\Delta - \gamma) \tilde{\rho}_{21} - i(\Omega + G \tilde{\rho}_{21})(\rho_{22} - \rho_{11}), \quad (8b)$$

where $\Delta \equiv \omega_L - \epsilon + \delta \omega$ is the effective detuning parameter (including the Lamb shift), $\tilde{\rho}_{12} = (\tilde{\rho}_{21})^* = \rho_{12} e^{-i\omega_L t}$ are the coherence elements transformed to a frame oscillating with the external field, $\Omega = (1 + r_\omega) \mathbf{d} \cdot \mathbf{E}^{\text{ext}} / \tilde{\epsilon} \hbar$ is the Rabi frequency, renormalized from its free space value $\mathbf{d} \cdot \mathbf{E}^{\text{ext}} / \hbar$, and $G = \omega_L^2 \mu_0 \mathbf{d} \cdot \mathcal{G}_\omega^{\text{ref}}(\mathbf{r}, \mathbf{r}) \cdot \mathbf{d} / \tilde{\epsilon} \hbar$ is a feedback parameter accounting for the TLA self-interaction mediated by the graphene sheet. Neglecting retardation and nonlocal effects, $\mathcal{G}_\omega(\mathbf{r}, \mathbf{r})$ conveniently admits closed-form expressions that we use here to describe the atom-graphene interaction over a range of parameters (see Supplemental Material [29]). Incidentally, the dephasing γ in Eqs. (8) is phenomenologically generalized to include additional possible decoherence channels, such that $\gamma \rightarrow \Gamma/2$ when relaxation occurs purely due to spontaneous emission.

The physics of Eqs. (8) has been extensively discussed in the context of semiconductor quantum dot (SQD)-metal nanoparticle (MNP) hybrid systems [6,7,9–11], and we summarize the role of the parameters: The TLA is driven at the effective Rabi frequency Ω , accounting for the external field and its reflection from the nanophotonic element (here the graphene sheet); meanwhile, the induced dipole

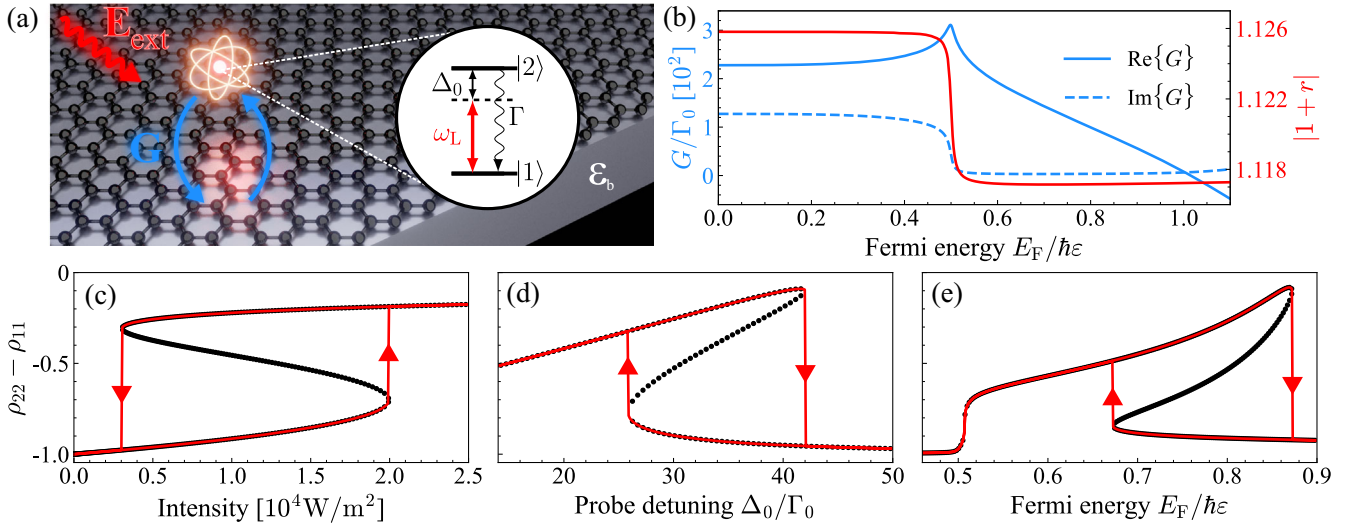


FIG. 1. Optical bistability in an atom interfacing graphene. (a) Schematic illustration of a two-level atom with ground state $|1\rangle$ and excited state $|2\rangle$ placed at a distance z above an extended graphene sheet encapsulated in media with dielectric permittivity ϵ_a above and ϵ_b below. (b) Self-interaction parameter G (left vertical axis) governing the dynamics of a TLA with transition energy $\hbar\epsilon = 1.0$ eV and vacuum decay rate Γ_0 placed $z = 12$ nm above a graphene sheet as the Fermi energy E_F is varied, while the reflection coefficient r for normal incidence (right axis) enters the effective Rabi frequency Ω . (c)–(e) The steady-state TLA population difference $Z = \rho_{22} - \rho_{11}$ is plotted in red curves corresponding to time-domain simulations obtained by adiabatically sweeping (c) the external field intensity I^{ext} at a distance $z = 17$ nm, (d) the detuning $\Delta_0 = \omega_L - \epsilon$ at $z = 17$ nm, and (e) the Fermi energy at $z = 12$ nm, and exhibit hysteresis indicated by the arrows; black dots correspond to solutions of Eq. (9). Unless explicitly varied, the results presented in (b)–(e) correspond to parameters $\epsilon_a = 1$, $\epsilon_b = 1.6$, $I^{ext} = 10 \text{ kW/m}^2$, $\hbar\Delta_0 = 8 \text{ } \mu\text{eV}$, and $E_F = 0.51 \text{ eV}$, while the TLA decay rate and transition dipole moment are $\Gamma_0 \approx 0.38 \text{ ns}^{-1}$ and $d = 1e \cdot \text{nm}$, respectively, and the broadening associated with inelastic scattering in graphene is $\hbar\tau^{-1} = 0.01 \text{ eV}$.

$\hat{d}\tilde{\rho}_{21}e^{-i\omega_L t} + \text{c.c.}$ produces a field that is reflected back on itself by the graphene sheet to modify the TLA transition frequency $\Delta \rightarrow \Delta + \text{Re}\{G\}(\rho_{22} - \rho_{11})$ and dephasing rate $\gamma \rightarrow \gamma + \text{Im}\{G\}(\rho_{22} - \rho_{11})$. The self-interaction term G thus endows the TLA response with an additional nonlinearity determined by geometric considerations (e.g., the separation distance) and the intrinsic optical properties of the nanophotonic environment, which are difficult to tune actively in SQD-MNP hybrids. The Lamb shift and Purcell enhancement introduce further sensitivity to changes in the local photonic density of states, but are often neglected in theoretical works describing similar systems. Here, minor changes to the Fermi energy E_F allow the graphene sheet to modulate the parameter G —which mediates the driven TLA self-interaction and quantum electrodynamic effects—and also (to a lesser extent) the effective Rabi frequency Ω in the spectral neighborhood of the $2E_F$ interband transition, as shown in Fig. 1(b) for a dipole oriented parallel to the graphene sheet.

Under steady-state conditions $\dot{\hat{\rho}} = 0$, Eqs. (8) yield

$$\frac{4\gamma}{\Gamma}|\Omega|^2 = -\frac{Z+1}{Z}[(\Delta - \text{Re}\{G\}Z)^2 + (\gamma - \text{Im}\{G\}Z)^2], \quad (9)$$

a third-order polynomial in the TLA population difference $Z \equiv \rho_{22} - \rho_{11}$ that admits up to three real solutions. The

nonlinearity introduced by the feedback parameter G thus renders the TLA bistable when three distinct solutions to Eq. (9) can be realized, two of which are stable.

External control over optical bistability is explored in Figs. 1(c)–1(e), where solutions of Eq. (9) are plotted as black dots and superimposed red curves indicate direct time-domain solutions of Eqs. (8) in the steady state obtained by adiabatically sweeping the impinging light intensity in Fig. 1(c), spectral detuning in Fig. 1(d), and graphene Fermi energy in Fig. 1(e). Time-domain solutions reveal hysteresis loops that are sensitive to the direction of change in the external parameters considered, and thus access different bistable regimes of the TLA population. As the control parameters are varied, pairs of steady state solutions appear or disappear at fold bifurcation points, around which small variations in the control parameter can dramatically change the population difference; such bifurcations can be deemed “catastrophic” [41,42]. Qualitatively similar optical bistability and hysteresis loops have been observed in experimental studies of dilute Rydberg gases when varying the intensity or frequency of the impinging laser field [43], while the graphene-atom system enables *in situ* reversible optoelectronic tuning of the TLA state by varying the graphene Fermi energy, in qualitative agreement with predictions for a driven TLA near a tunable indium tin oxide film [11]. The Fermi energies considered in Fig. 1 are commensurate with those attained in experiments involving top-gated graphene [23,25,26].

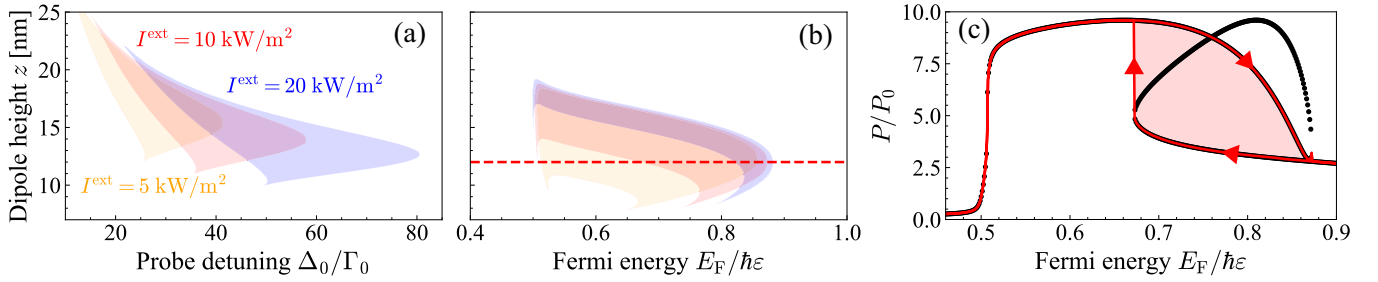


FIG. 2. Regimes of optical bistability. (a) Regions of bistability indicated by the discriminant of Eq. (9) for various impinging light intensities I^{ext} as a function of probe detuning Δ_0 and graphene-TLA distance z . (b) Same as (a) but sweeping the Fermi energy E_F at fixed detuning. (c) Normalized average radiation power as a function of E_F for $z = 12$ nm, corresponding to the horizontal dashed line in (b). TLA and graphene parameters are the same as those in Fig. 1 unless otherwise specified.

Optoelectronic bistability in the TLA-graphene system is associated with a positive discriminant of the third-order polynomial in Eq. (9), which we map over the TLA-graphene separation z at various impinging light intensities while varying detuning in Fig. 1(a) and Fermi energy in Fig. 1(b). In the former situation, the light intensity primarily shifts the spectral window where bistability emerges, while in the latter case the intensity affects the range of separations. Linear stability analysis reveals that the stability of the steady-state solutions in Figs. 2(a) and 2(b) are indeed comprised of two stable solutions and one unstable solution (see Supplemental Material [29] for details). The bistable state of the TLA-graphene system can be observed in the total normalized radiation power from the TLA, obtained by integrating the dipole radiation pattern over all angles [40], and presented in Fig. 2(c) at a separation distance of $z = 12$ nm and detuning $\hbar\Delta_0 = 8 \mu\text{eV}$ corresponding to the horizontal dashed line in Fig. 2(b). Notably, by tuning E_F in graphene, the radiation power can achieve a tenfold enhancement for the parameters under consideration, while the hysteresis behavior presents a clear signature of atomic bistability.

The results of Figs. 1 and 2 are obtained for TLA parameters commensurate with quantum dots, with large transition dipole moments enabling strong self-interaction at distances $\gtrsim 10$ nm from the graphene sheet. Qualitatively similar atomic bistability manifests in more atomlike two-level systems with weaker dipole moments when they are placed closer to graphene, as we show in the Supplemental Material [29] for the case of rare-earth erbium ions emitting near 0.8 eV (at the 1.5 μm telecommunications wavelength) that have been employed in recent experiments to demonstrate the ability of graphene to modulate spontaneous emission of nearby quantum light emitters [25,26]. The generality of the proposed mechanism for atomic bistability could thus allow different classes of TLA to be explored in experiment, where the compatible TLA transition energies are mainly determined by the achievable Fermi energy in a graphene device and the TLA dipole moment sets the separation distance.

Atomic bistability also manifests in the spectrum of fluorescent light emitted by the TLA, obtained from the first-order correlation function of the emitted field [44]. Typically, for weak excitation, incident and fluorescent light frequencies coincide, and the incoherent spectrum forms a single Rayleigh peak; under strong driving, the TLA spectrum exhibits a large central peak and two sidebands—the so-called Mollow triplet [45]. As the upper and lower TLA population branches are accessed by tuning the graphene Fermi energy in Fig. 3(a), the fluorescence spectrum in the right panel of Fig. 3(b) exhibits a bistable response, with states distinguished by variations spanning a single Rayleigh peak to the Mollow triplet at the indicated points. Note that for an isolated atom, sidebands split continuously from the Rayleigh peak as the incident field intensity increases, in a manner roughly equivalent to a second-order phase transition [46,47]. In contrast, the discontinuous change in the fluorescence spectrum exhibited by the TLA-graphene system when tuning E_F (e.g., between regions I and II or III and IV) is reminiscent of first-order phase transitions in a system at thermal equilibrium.

The second-order correlation function $g^{(2)}(\tau)$ associated with the emitted light at selected points is presented in the left panel of Fig. 3(b), presenting antibunching for vanishing time delay $\tau = 0$ while approaching unity as $\tau \rightarrow \infty$ [14,44], either monotonically evolving or rapidly oscillating between these limits depending on the bistability region. Analogous to the resonance fluorescence spectrum, the transient statistics of the emitted light can be abruptly modified by traversing the hysteresis curve (e.g., from region III to IV).

The characteristic timescale τ_s on which a TLA in a bistable state can be brought from one stable branch to another is an important metric for optical switching applications [8,48], and has also been exploited to herald phase transitions in dilute Rydberg ensembles [43]. While approaching a bifurcation point (see vertical arrows in Fig. 1), the system becomes increasingly slow at recovering from perturbations [41]. The slow-down of a bistable

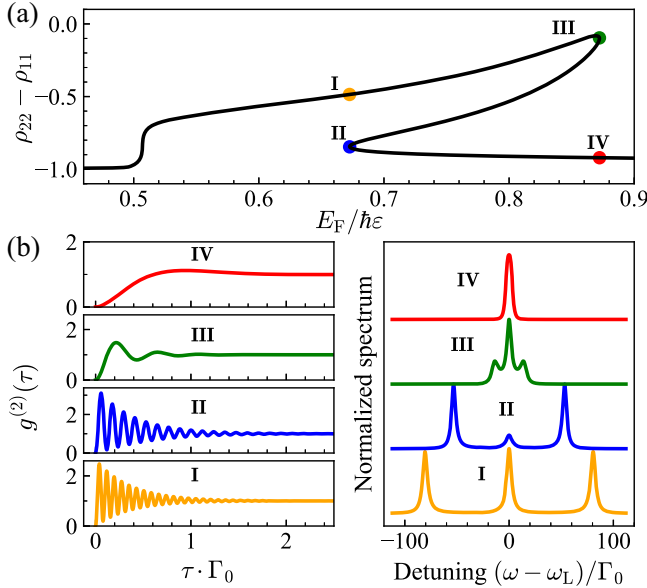


FIG. 3. Signatures of optical bistability in resonance fluorescence and antibunching. (a) Steady-state TLA population difference Z obtained from Eq. (9) plotted as a function of the graphene Fermi energy E_F when the TLA is $z = 12$ nm above the graphene sheet and driven at a frequency corresponding to $\Delta_0 = 8$ μeV by a field of intensity $I^{\text{ext}} = 10$ kW/m^2 . (b) The second-order correlation function $g^{(2)}(\tau)$ (left panel) and resonance fluorescence spectra (right panel) are presented as functions of delay time τ and detuning $\omega - \omega_L$, respectively, for system parameters indicated by the color-coordinated points I–IV in panel (a).

device at such critical points is characterized by a power law in the control parameter (e.g., E_F , I^{ext} , or Δ_0) triggering a transition from lower to upper stable branches along the hysteresis curve. For instance, when moving from point IV to I in Fig. 3, a linear stability analysis reveals that critical slow-down occurs at point II, such that $\tau_s \propto |E_F - E_F^c|^{-\alpha}$, where τ_s is defined here as the time to reach maximum population inversion [48], E_F^c is the critical Fermi energy, and $\alpha \approx 0.5$ is the critical exponent (see Supplemental Material [29] for details). Interestingly, critical exponents $\alpha \approx 0.5$ are obtained independently of the control parameter, suggesting a universal critical slow-down of the bistable transition; these findings are corroborated by reports of cooperative interactions among quantum emitters, e.g., in a theoretical study of an optically driven TLA coupled with a plasmonic nanoparticle [48], or in measurements of a dilute Rydberg gas ensemble [43].

In summary, we propose to harness the interband transition threshold in graphene to achieve electro-optical control of atomic bistability. Here, optical bistability emerges from the self-interaction of the atomic transition dipole with its image in the graphene sheet, which also influences the Purcell effect and Lamb shift, leading to a rich interplay between the driven optical nonlinearity and quantum electrodynamic response as the Fermi energy is modulated. We show that the bistability and hysteresis

behavior resulting from the atom-graphene interaction can be observed in the light scattered by the atom, specifically in the radiated power, resonance fluorescence spectrum, and photon statistics. In particular, electrical tuning of the graphene sheet can trigger critical slow-down of the steady-state approach in the TLA dynamics, which is heralded in the scattering spectrum by a discontinuous quench of the sidebands or Rayleigh peak in the Mollow triplet when traversing hysteresis loops. The proposed concept of electrically tuning optically-driven atom-graphene interactions constitutes a versatile platform for fundamental explorations in atomic physics and quantum nano-optics. Application perspectives for the present scheme include controllable quantum light sources and integrated photonic memory devices [49], while external tuning of bistability in the cooperative interactions between multiple atoms holds enticing possibilities for quantum entanglement [17] and multiphoton generation [50].

The authors thank Fabio Raspanti, P. A. D. Gonçalves, Sebastian Hofferberth, N. Asger Mortensen, and Klaus Mølmer for insightful and enjoyable discussions. J. D. C. is a Sapere Aude research leader supported by VILLUM FONDEN (Grant No. 16498) and Independent Research Fund Denmark (Grant No. 0165-00051B).

*cox@mci.sdu.dk

- [1] A. Streltsov, G. Adesso, and M. B. Plenio, *Rev. Mod. Phys.* **89**, 041003 (2017).
- [2] P. Lodahl, S. Mahmoodian, and S. Stobbe, *Rev. Mod. Phys.* **87**, 347 (2015).
- [3] D. E. Chang, J. S. Douglas, A. González-Tudela, C.-L. Hung, and H. J. Kimble, *Rev. Mod. Phys.* **90**, 031002 (2018).
- [4] W. Zhang, A. O. Govorov, and G. W. Bryant, *Phys. Rev. Lett.* **97**, 146804 (2006).
- [5] A. Ridolfo, O. Di Stefano, N. Fina, R. Saija, and S. Savasta, *Phys. Rev. Lett.* **105**, 263601 (2010).
- [6] R. D. Artuso and G. W. Bryant, *Nano Lett.* **8**, 2106 (2008).
- [7] R. D. Artuso and G. W. Bryant, *Phys. Rev. B* **82**, 195419 (2010).
- [8] F. Carreño, M. A. Antón, and E. Paspalakis, *J. Appl. Phys.* **124**, 113107 (2018).
- [9] A. V. Malyshev and V. A. Malyshev, *Phys. Rev. B* **84**, 035314 (2011).
- [10] A. V. Malyshev, *Phys. Rev. A* **86**, 065804 (2012).
- [11] J. M. Arrieta, *Modelling of Plasmonic and Graphene Nano-devices* (Springer, New York, 2014).
- [12] M. A. Antón, F. Carreño, S. Melle, O. G. Calderón, E. Cabrera-Granado, J. Cox, and M. R. Singh, *Phys. Rev. B* **86**, 155305 (2012).
- [13] F. Carreño, M. A. Antón, and F. Arrieta-Yáñez, *Phys. Rev. B* **88**, 195303 (2013).
- [14] A. Mohammadzadeh and M. F. Miri, *Phys. Rev. B* **99**, 115440 (2019).
- [15] P. A. D. Gonçalves and N. M. R. Peres, *An Introduction to Graphene Plasmonics* (World Scientific, Singapore, 2016).

- [16] F. H. L. Koppens, D. E. Chang, and F. J. García de Abajo, *Nano Lett.* **11**, 3370 (2011).
- [17] A. Manjavacas, S. Thongrattanasiri, D. E. Chang, and F. J. García de Abajo, *New J. Phys.* **14**, 123020 (2012).
- [18] E. Foratí, G. W. Hanson, and S. Hughes, *Phys. Rev. B* **90**, 085414 (2014).
- [19] C.-H. Chang, N. Rivera, J. D. Joannopoulos, M. Soljačić, and I. Kaminer, *ACS Photonics* **4**, 3098 (2017).
- [20] F. J. García de Abajo, *ACS Photonics* **1**, 135 (2014).
- [21] J. D. Cox and F. J. García de Abajo, *Phys. Rev. Lett.* **121**, 257403 (2018).
- [22] F. Wang, Y. Zhang, C. Tian, C. Girit, A. Zettl, M. Crommie, and Y. R. Shen, *Science* **320**, 206 (2008).
- [23] C.-F. Chen, C.-H. Park, B. W. Boudouris, J. Horng, B. Geng, C. Girit, A. Zettl, M. F. Crommie, R. A. Segalman, S. G. Louie, and F. Wang, *Nature (London)* **471**, 617 (2011).
- [24] J. Lee, W. Bao, L. Ju, P. J. Schuck, F. Wang, and A. Weber-Bargioni, *Nano Lett.* **14**, 7115 (2014).
- [25] K. J. Tielrooij, L. Orona, A. Ferrier, M. Badioli, G. Navickaite, S. Coop, S. Nanot, B. Kalinic, T. Cesca, L. Gaudreau, Q. Ma, A. Centeno, A. Pesquera, A. Zurutuza, H. de Riedmatten, P. Goldner, F. J. García de Abajo, P. Jariillo-Herrero, and F. H. L. Koppens, *Nat. Phys.* **11**, 281 (2015).
- [26] D. Cano, A. Ferrier, K. Soundarapandian, A. Reserbat-Plantey, M. Scarafagio, A. Tallaire, A. Seyeux, P. Marcus, H. de Riedmatten, P. Goldner, F. H. L. Koppens, and K.-J. Tielrooij, *Nat. Commun.* **11**, 4094 (2020).
- [27] M. O. Scully and M. S. Zubairy, *Quantum Optics* (Cambridge University Press, Cambridge, 1997).
- [28] T. V. C. Antão and N. M. R. Peres, *Int. J. Mod. Phys. B* **35**, 2130007 (2021).
- [29] See Supplemental Material at <http://link.aps.org/supplemental/10.1103/PhysRevLett.129.253602> for details on the theoretical formalism describing the dynamics and fluorescence of an optically driven two-level atom interacting with a graphene sheet, stability analysis of steady-state solutions to the optical Bloch equations, and simulations of bistability for an alternative two-level atom parametrization, which includes Refs. [30–38].
- [30] D. Dzsojjan, J. Kästel, and M. Fleischhauer, *Phys. Rev. B* **84**, 075419 (2011).
- [31] U. Hohenester, *Nano and Quantum Optics* (Springer, New York, 2020).
- [32] P. A. D. Gonçalves, *Plasmonics and Light–Matter Interactions in Two-Dimensional Materials and in Metal Nanostructures: Classical and Quantum Considerations* (Springer Nature, Switzerland AG, 2020).
- [33] N. D. Mermin, *Phys. Rev. B* **1**, 2362 (1970).
- [34] U. Hoepe, C. Wolff, J. Küchenmeister, J. Niegemann, M. Drescher, H. Benner, and K. Busch, *Phys. Rev. Lett.* **108**, 043603 (2012).
- [35] M. Abramowitz and I. A. Stegun, *Handbook of Mathematical Functions with Formulas, Graphs, and Mathematical Tables* (US Government printing office, Washington, DC, 1948), Vol. 55.
- [36] M. Orszag, *Quantum Optics: Including Noise Reduction, Trapped Ions, Quantum Trajectories, and Decoherence* (Springer, New York, 2016).
- [37] L. Lugiato, F. Prati, and M. Brambilla, *Nonlinear Optical Systems* (Cambridge University Press, Cambridge, England, 2015).
- [38] R. Bonifacio and P. Meystre, *Opt. Commun.* **29**, 131 (1979).
- [39] S. Scheel and S. Y. Buhmann, *Acta Phys. Slovaca* **58**, 675 (2008).
- [40] L. Novotny and B. Hecht, *Principles of Nano-Optics* (Cambridge University Press, Cambridge, England, 2012).
- [41] M. Scheffer, J. Bascompte, W. A. Brock, V. Brovkin, S. R. Carpenter, V. Dakos, H. Held, E. H. V. Nes, M. Rietkerk, and G. Sugihara, *Nature (London)* **461**, 53 (2009).
- [42] S. H. Strogatz, *Nonlinear Dynamics and Chaos: With Applications to Physics, Biology, Chemistry, and Engineering* (CRC Press, 2018).
- [43] C. Carr, R. Ritter, C. G. Wade, C. S. Adams, and K. J. Weatherill, *Phys. Rev. Lett.* **111**, 113901 (2013).
- [44] P. Meystre and M. Sargent, *Elements of Quantum Optics* (Springer Science & Business Media, New York, 2007).
- [45] B. R. Mollow, *Phys. Rev.* **188**, 1969 (1969).
- [46] R. Bonifacio and L. A. Lugiato, *Opt. Commun.* **19**, 172 (1976).
- [47] R. Bonifacio and L. A. Lugiato, *Phys. Rev. A* **18**, 1129 (1978).
- [48] B. S. Nugroho, A. A. Iskandar, V. A. Malyshev, and J. Knoester, *J. Chem. Phys.* **139**, 014303 (2013).
- [49] C. Valagiannopoulos, A. Sarsen, and A. Alù, *IEEE Trans. Antennas Propag.* **69**, 7720 (2021).
- [50] A. González-Tudela, V. Paulisch, H. J. Kimble, and J. I. Cirac, *Phys. Rev. Lett.* **118**, 213601 (2017).